



## Article

# State of Charge Estimation of Lithium Battery Utilizing Strong Tracking H-Infinity Filtering Algorithm

Tianqing Yuan <sup>1,2</sup>, Yang Liu <sup>1,2</sup>, Jing Bai <sup>3</sup> and Hao Sun <sup>4,\*</sup>

<sup>1</sup> Key Laboratory of Modern Power System Simulation and Control & Renewable Energy Technology, Ministry of Education, Northeast Electric Power University, Jilin 132012, China; 20192929@neepu.edu.cn (T.Y.)

<sup>2</sup> Department of Electrical Engineering, Northeast Electric Power University, Jilin 132012, China

<sup>3</sup> Yuda Engineering (Jilin) Co., Ltd., Siping 136000, China

<sup>4</sup> College of Information and Control Engineering, Jilin Institute of Chemical Technology, Jilin 132022, China

\* Correspondence: sunhao218@jlict.edu.cn

**Abstract:** The ability to quickly and accurately estimate the state of charge (SOC) of lithium batteries is a key function of the battery management system (BMS). To enhance the accuracy of SOC estimation for lithium batteries, we propose a method that combines the dynamic factor recursive least squares (DFFRLS) algorithm and the strong tracking H-infinity filtering (STF-HIF) algorithm. To address the issue of fixed forgetting factors in recursive least squares (RLS) that struggle to maintain both fast convergence and stability in battery parameter identification, we introduce dynamic forgetting factors. This approach adjusts the forgetting factor based on the residuals between the model's estimated and actual values. To improve the H-infinity filtering (HIF) algorithm's poor performance in tracking sudden state changes, we propose a combined STF-HIF algorithm, integrating HIF with strong tracking filtering (STF). Simulation experiments indicate that, compared to the HIF algorithm, the STF-HIF algorithm achieves a maximum absolute SOC estimation error (MaxAE) of 0.69%, 0.72%, and 1.22%, with mean absolute errors (MAE) of 0.27%, 0.25%, and 0.38%, and root mean square errors (RMSE) of 0.33%, 0.30%, and 0.46% under dynamic stress testing (DST), federal urban driving schedules (FUDS), and Beijing dynamic stress testing (BJDST) conditions, respectively.



**Citation:** Yuan, T.; Liu, Y.; Bai, J.; Sun, H. State of Charge Estimation of Lithium Battery Utilizing Strong Tracking H-Infinity Filtering Algorithm. *Batteries* **2024**, *10*, 388. <https://doi.org/10.3390/batteries10110388>

Academic Editor: Seiji Kumagai

Received: 6 September 2024

Revised: 31 October 2024

Accepted: 2 November 2024

Published: 4 November 2024



**Copyright:** © 2024 by the authors. Licensee MDPI, Basel, Switzerland. This article is an open access article distributed under the terms and conditions of the Creative Commons Attribution (CC BY) license (<https://creativecommons.org/licenses/by/4.0/>).

## 1. Introduction

To tackle the challenge of traditional energy shortages, the government has actively encouraged the development of new energy technologies through supportive policies and initiatives, including the demonstration and widespread adoption of new energy vehicles (NEVs) [1]. In this context, the advancement of NEV technologies has become particularly crucial. Lithium batteries, renowned for their high energy density and long lifespan, are extensively used in the NEV sector [2,3]. The reliable performance of NEVs heavily depends on a robust and secure BMS that monitors and safeguards the batteries. One of the most important factors within the BMS is the SOC. As a result, accurately estimating the key states of lithium batteries during operation remains a significant challenge. The SOC is a vital indicator of a battery's condition, and the ability to quickly and precisely estimate the SOC is crucial for optimizing energy management in electric vehicles [4,5].

High-precision model parameter identification, essential for battery SOC estimation, can be divided into offline and online types. Offline parameter identification cannot adapt parameters dynamically based on data changes, rendering it impractical for real-world applications. Compared to offline methods, online parameter identification is more accurate and widely applicable. The RLS algorithm is the most widely used method for online parameter identification [6–8]. It offers fast convergence and high identification accuracy.

However, as input data increases, the algorithm can experience data saturation, preventing it from acquiring information from new data and reducing parameter identification accuracy. To address this shortcoming, researchers have proposed a series of improved algorithms [9–11]. In reference [12], the RLS algorithm with a forgetting factor was used for bias compensation, enhancing the parameter identification accuracy for colored noise data. Reference [13] utilized the forgetting factor recursive least squares (FFRLS) method to identify parameters of second-life battery models. Continuous adjustment of the forgetting factor allowed better tracking of battery aging characteristics. In reference [14], a high-order sliding mode differentiator combined with the RLS algorithm was used to identify battery model parameters. This method enabled online identification of battery model parameters and provided some noise tolerance. Besides RLS and its derived algorithms, genetic algorithms [15], Kalman filter algorithms [16], and the maximum likelihood function method [17] are also commonly used for online identification of battery model parameters.

Currently, the commonly used methods for estimating the SOC of lithium batteries include direct measurement, model-based methods, and intelligent algorithm-based methods. This method is convenient and straightforward. However, the open-circuit voltage method has a drawback: it requires a resting period to measure accurately, which is impractical during use. The ampere-hour integration method also has limitations, such as its reliance on an accurate initial state of charge (SOC) and susceptibility to current drift, noise, and aging. In practice, SOC estimation often combines the ampere-hour integration and open-circuit voltage methods. During battery use, the ampere-hour integration method measures the discharged capacity, while the open-circuit voltage method is used during rest periods. This combination allows for an economical and quick estimation of SOC, making it a well-established solution.

Among model-based SOC estimation methods [18–20], the approach based on the HIF algorithm employs the minimax error criterion. This approach provides high SOC estimation accuracy and robustness under unknown noise statistical characteristics. In recent years, SOC estimation based on HIF has garnered significant attention from scholars. Reference [21] established an adaptive HIF algorithm based on fractional-order and capacity compensation models to achieve high-precision SOC estimation. However, this approach increases model complexity, complicates hardware implementation, and introduces inevitable time delays, reducing the real-time performance of SOC estimation. Reference [22] proposed the  $H_\infty$  Extended Kalman Filter (HEKF) algorithm based on robust control theory. It estimates SOC while simultaneously updating model parameters like ohmic resistance in real time, enhancing convergence speed and robustness. However, it still suffers from errors inherent in linearizing nonlinear systems during the EKF process. Reference [23] mapped battery model parameters based on voltage, current, temperature, and aging state using neural networks. It then employed adaptive HIF to reduce estimation jitter and improve accuracy. This method requires extensive offline data for model training, which also diminishes the real-time performance of SOC estimation. Reference [24] combined equivalent circuit models with data-driven autoregressive models to develop a multi-scale SOC estimation method based on HIF, enhancing estimation accuracy from the perspective of battery modeling. However, the lack of noise assumptions during estimation is impractical, and the filtering performance is overly sensitive to parameter design, complicating hardware debugging. Reference [25] designed a Finite Time  $H_\infty$  Observer (FTHIO) based on the recursive least squares method to improve SOC estimation accuracy. This approach sacrifices algorithm generality for faster convergence, and its practical applicability requires further validation. Estimation methods based on intelligent algorithms excel [26,27] at handling nonlinear problems. However, they require a large amount of training data and are time-consuming. Conventional SOC estimation methods, as discussed in references [28–30], have proposed various approaches, but each has its limitations.

To meet the high-precision requirements of SOC estimation, this paper adopts the DF-FFRLS method for online identification of model parameters, ensuring model accuracy [31,32].

Based on the HIF algorithm, the STF algorithm is introduced, forming the STF-HIF. The proposed STF-HIF algorithm improves the gain matrix based on the relevant information from the estimated residual sequence, enabling the system to track sudden state changes and achieve more accurate estimation results.

## 2. Equivalent Circuit Model of a Lithium-Ion Battery

The lithium batteries equivalent circuit model is an empirical model. The Thevenin model, known for its simple structure and effective reflection of the battery's dynamic characteristics, has garnered significant attention [33,34]. Therefore, this paper selects the second-order RC Thevenin model to study lithium battery SOC estimation methods. The second-order RC Thevenin model is illustrated in Figure 1.

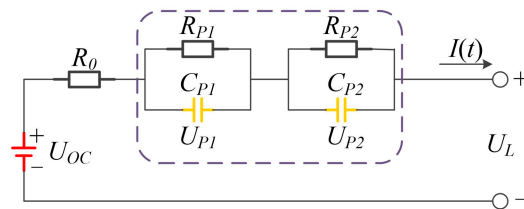


**Figure 1.** Second-order RC Thevenin model.

In Figure 1,  $U_{OC}$ ,  $U_L$ ,  $I(t)$ , and  $R_0$  represent the battery's open-circuit voltage, terminal voltage, operating current, and ohmic resistance, respectively.  $R_{P1}$  and  $C_{P1}$  represent the electrochemical polarization phenomenon occurring at the positive and negative electrodes inside the battery, while  $R_{P2}$  and  $C_{P2}$  represent the concentration gradient effect.  $U_{P1}$  and  $U_{P2}$  are the voltages across the  $R_{P1}$ ,  $C_{P1}$  and  $R_{P2}$ ,  $C_{P2}$  loops, respectively. From Figure 2, we can derive the following:

$$U_L = U_{OC}(SOC) - I(t)R_0 - U_{P1} - U_{P2} \quad (1)$$

$$\begin{cases} \frac{dU_{P1}}{dt} = -\frac{U_{P1}}{R_{P1}C_{P1}} + \frac{I}{C_{P1}} \\ \frac{dU_{P2}}{dt} = -\frac{U_{P2}}{R_{P2}C_{P2}} + \frac{I}{C_{P2}} \end{cases} \quad (2)$$

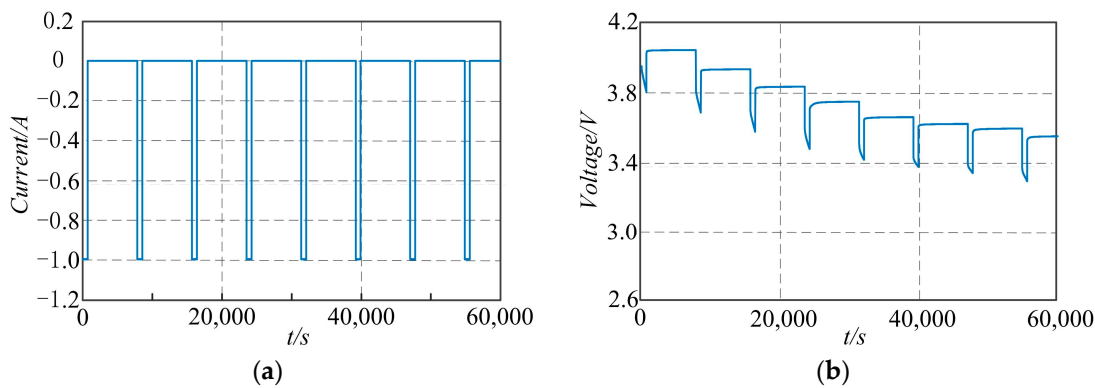


**Figure 2.** (a) Current during the HPPC test; (b) Voltage of HPPC test.

For the selected equivalent model, choosing  $SOC$ ,  $U_{P1}$  and  $U_{P2}$  as state variables, the battery's state equation can be obtained, as shown in Equation (3).

$$\begin{bmatrix} SOC(k+1) \\ U_{P1}(k+1) \\ U_{P2}(k+1) \end{bmatrix} = \begin{bmatrix} 1 & 0 & 0 \\ 0 & A & 0 \\ 0 & 0 & B \end{bmatrix} \begin{bmatrix} SOC(k) \\ U_{P1}(k) \\ U_{P2}(k) \end{bmatrix} + \begin{bmatrix} -\frac{\eta\Delta t}{Q} \\ R_{P1}(1-A) \\ R_{P2}(1-B) \end{bmatrix} I(k) + w(k) \quad (3)$$

In the equation:  $SOC(k)$  indicates the battery's state of charge at time  $k$ ;  $\eta$  denotes the coulombic efficiency of the battery;  $\Delta t$  represents the system's sampling period; and  $Q$  stands for the battery's nominal capacity. The state variables A and B are defined as follows:

$$\begin{cases} A = e^{-\frac{\Delta t}{R_1 C_{P1}}} \\ B = e^{-\frac{\Delta t}{R_2 C_{P2}}} \end{cases} \quad (4)$$

Additionally, the battery's output equation can be expressed as

$$U_L(k) = U_{OC}(SOC(k)) - R_0 I(k) - U_{P1}(k) - U_{P2}(k) + v_k \quad (5)$$

In the equation:  $I(k)$  represents the current at time  $k$ ; and  $w(k)$  and  $v(k)$ , respectively, represent the process noise and measurement noise of the system.

### 3. Online Identification of Model Parameters

This study uses the cylindrical battery model INR 18650-20R as the experimental subject. INR 18650-20R is a lithium-ion battery manufactured by Samsung SDI in Korea which has a nominal capacity of 2 Ah and a cutoff voltage range of 2.5 to 4.2 V. The basic characteristics experiments for this battery include the hybrid pulse power characterization (HPPC) test, with data sourced from the publicly available dataset from the University of Maryland [35]. The specific experimental steps are as follows:

- (1) Maintain an ambient temperature of 25 °C, and continuously discharge or charge the battery using a 0.2 C current pulse.
- (2) Every time 10% of the SOC is either charged or discharged, allow the battery to rest for 10 min.
- (3) Repeat step (2) until the voltage reaches the cutoff limit for charging or discharging.
- (4) Record the terminal voltages during both the charging and discharging rest periods, and determine the values based on the SOC at those times.

Figure 2 illustrates the voltage and current of the University of Maryland 18650 battery during the HPPC test conducted at 25 °C.

#### 3.1. OCV-SOC Characteristic Curve

The OCV-SOC characteristic curve generally necessitates the use of online parameter identification and estimation algorithms. Therefore, accurately depicting the relationship between OCV and SOC is a vital step in SOC estimation. To acquire the OCV values, the battery needs to rest for an adequate period. In this research, we segmented the battery's SOC range from 0 to 1 into 11 equal intervals and carried out HPPC experiments to determine the OCV-SOC relationship, as illustrated in Table 1.

**Table 1.** OCV-SOC correspondence.

SOC (%)	OCV(V)	SOC (%)	OCV(V)
0	3.385	60	3.753
10	3.467	70	3.893
20	3.555	80	3.940
30	3.599	90	4.050
40	3.625	100	4.166
50	3.664		

The experimental data on the OCV-SOC function relationship were fitted using 4th, 5th, 6th, and 7th-degree polynomials. The resulting fitting curves are displayed in Figure 3. The goodness of fit for these polynomial functions is typically assessed using the multiple correlation coefficient ( $R^2$ ). The closer the  $R^2$  value is to 1, the better the fit. The  $R^2$  values for the 4th to 7th-degree fitting functions are presented in Table 2.

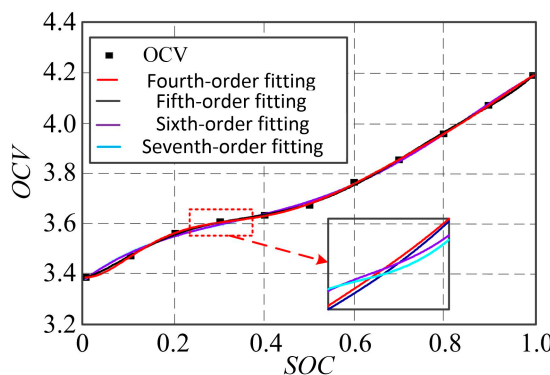


**Figure 3.** OCV-SOC curve chart.

**Table 2.**  $R^2$  values for the 4th to 7th-degree fitting functions.

Order	Fourth	Fifth	Sixth	Seventh
$R^2$	0.997	0.997	0.999	0.999

From Figure 3 and Table 2, it can be observed that the 4th to 7th-degree fitting functions nearly overlap. The  $R^2$  values for the 6th and 7th-degree fitting functions are identical and closest to 1. Considering that higher-degree functions increase computational complexity, this study selects the 6th-degree polynomial fit, as shown in Equation (6).

$$\text{OCV} = 20.229\text{SOC}^6 - 61.776\text{SOC}^5 + 68.888\text{SOC}^4 - 32.756\text{SOC}^3 + 5.639\text{SOC}^2 + 0.559\text{SOC} + 3.384 \quad (6)$$

### 3.2. Mathematical Derivation of Model Least Squares Method

According to the second-order RC Thevenin model,  $U_{OC}$  can be represented as shown in Equation (7).

$$U_{OC} = \left( R_0 + \frac{R_{p1}}{R_{p1}C_{p1}s + 1} + \frac{R_{p2}}{R_{p2}C_{p2}s + 1} \right) I + U_L \quad (7)$$

Let the time constants be  $\tau_1 = R_{p1}C_{p1}$  and  $\tau_2 = R_{p2}C_{p2}$ , then Equation (7) becomes:

$$\begin{aligned} \tau_1 t_2 U_{oc}s^2 + (\tau_1 + t_2)U_{oc}s + U_{oc} &= (\tau_1 + t_2)U_L s + (R_0 + R_{p1} + R_{p2})I + \tau_1 t_2 R_0 I s^2 \\ &\quad + [R_0(t_1 + t_2) + R_{p1}t_2 + R_{p2}t_1]I s + \tau_1 t_2 U_L s^2 + U_L \end{aligned} \quad (8)$$

Define  $a = \tau_1 \tau_2$ ,  $b = \tau_1 + \tau_2$ ,  $c = R_0 + R_{p1} + R_{p2}$ ,  $d = R_0(\tau_1 + \tau_2) + R_{p1}\tau_2 + R_{p2}\tau_1$ , then Equation (8) can be simplified as follows:

$$aU_{oc}s^2 + bU_{oc}s + U_{oc} = aR_0 I s^2 + dI s + cI + aU_L s + bU_L s + U_L \quad (9)$$

Substituting  $s = [x(k) - x(k - 1)]/T$ ,  $s^2 = [x(k) - 2x(k - 1) + x(k - 2)]/T^2$  into Equation (9) for discretization, and rearranging, we obtain the following:

$$\begin{aligned} y(k) = U_{oc}(k) - U_L(k) &= k_1[U_{oc}(k - 1) - U_L(k - 1)] + k_2[U_{oc}(k - 2) - U_L(k - 2)] \\ &\quad + k_3I(k) + k_4I(k - 1) + k_5I(k - 2) \end{aligned} \quad (10)$$

In the equation:  $y(k)$  is the system output; and  $k_1, k_2, k_3, k_4$  and  $k_5$  are the identification parameters.

Let  $\theta = [k_1, k_2, k_3, k_4, k_5]^T$ ,  $\varphi(k) = [U_{OC}(k - 1) - U_L(k - 1), U_{OC}(k - 2) - U_L(k - 2), I(k), I(k - 1), I(k - 2)]^T$ . Then, Equation (10) can be expressed as follows:

$$y(k) = \varphi(k)^T \theta \quad (11)$$

In the equation,  $\theta$  is the parameter identification matrix.

### 3.3. Forgetting Factor Recursive Least Squares Method

As the number of samples increases, the RLS algorithm can experience severe filter saturation, preventing real-time tracking of time-varying parameters and weakening data correction capability. To address this, a forgetting factor  $\lambda$  ( $0.95 < \lambda < 1$ ) is introduced into the RLS identification algorithm. By applying the forgetting factor to old data, the weights of new and old data can be redistributed, thereby avoiding data redundancy and mitigating saturation issues. The specific recursive formulas for the FFRLS are as follows:

$$\begin{cases} \hat{\theta}(k) = \hat{\theta}(k-1) + K(k)(y(k) - \varphi^T(k)\hat{\theta}(k-1)) \\ K(k) = \frac{P(k-1)\varphi(k)}{\lambda + \varphi^T(k)P(k-1)\varphi(k)} \\ P(k) = \frac{1}{\lambda}[I - K(k)\varphi^T(k)]P(k-1) \end{cases} \quad (12)$$

In the equations:  $\varphi^T(k)\hat{\theta}(k-1)$  is the theoretical observation value at time  $k$ ;  $y(k)$  is the actual observation value at time  $k$ ;  $\varphi^T(k)$  is the transpose matrix at time  $k$ ;  $\hat{\theta}(k-1)$  is the coefficient matrix at time  $k-1$ ;  $K(k)$  is the gain factor of the algorithm;  $I$  is the identity matrix of corresponding dimensions; and  $P(k)$  is the error covariance matrix at time  $k$ .

The smaller the forgetting factor  $\lambda$ , the greater the weight of new data, which allows the recursion to better reflect the system's dynamic characteristics, improving tracking performance and algorithm convergence speed. Conversely, the larger the forgetting factor  $\lambda$ , the greater the weight of old data, biasing the recursion towards overall optimality. Although tracking performance declines, algorithm stability is enhanced. The DFFRLS method proposed in this paper can simultaneously maintain rapid convergence and stability of the algorithm.

### 3.4. Dynamic Forgetting Factor Recursive Least Squares Method

When using the FFRLS method for parameter identification, the forgetting factor  $\lambda$  is usually fixed [36]. Regardless of its value, this can affect the algorithm's stability and rapid convergence. To solve this issue and simultaneously maintain fast convergence and stability, a dynamic forgetting factor is incorporated into the RLS method. The forgetting factor is dynamically adjusted based on the real-time residuals between the identification results and actual values. The real-time residual at time  $k$  can be expressed as follows:

$$\varepsilon(k) = y(k) - \varphi^T(k)\theta(k-1) \quad (13)$$

The residual  $\varepsilon(k)$  is mainly caused by identification errors, with minimal impact from measurement noise. To ensure both rapid convergence and stability of the algorithm, the forgetting factor needs to be reduced in real-time when the residual  $\varepsilon(k)$  is large, thereby enhancing the algorithm's tracking speed and ensuring quick convergence. Conversely, when the residual  $\varepsilon(k)$  is small, the forgetting factor needs to be increased in real-time to incorporate previously recursively computed old data, thereby improving stability. The established correction formula for the forgetting factor  $\lambda$  is as follows:

$$\lambda(k) = \alpha + (1 - \alpha)e^{-\gamma\varepsilon(k)} \quad (14)$$

In the equation:  $\alpha$  is a value close to but less than 1; and  $\gamma$  is an adjustable positive parameter.

The flowchart for dynamic forgetting factor parameter identification is shown in Figure 4.

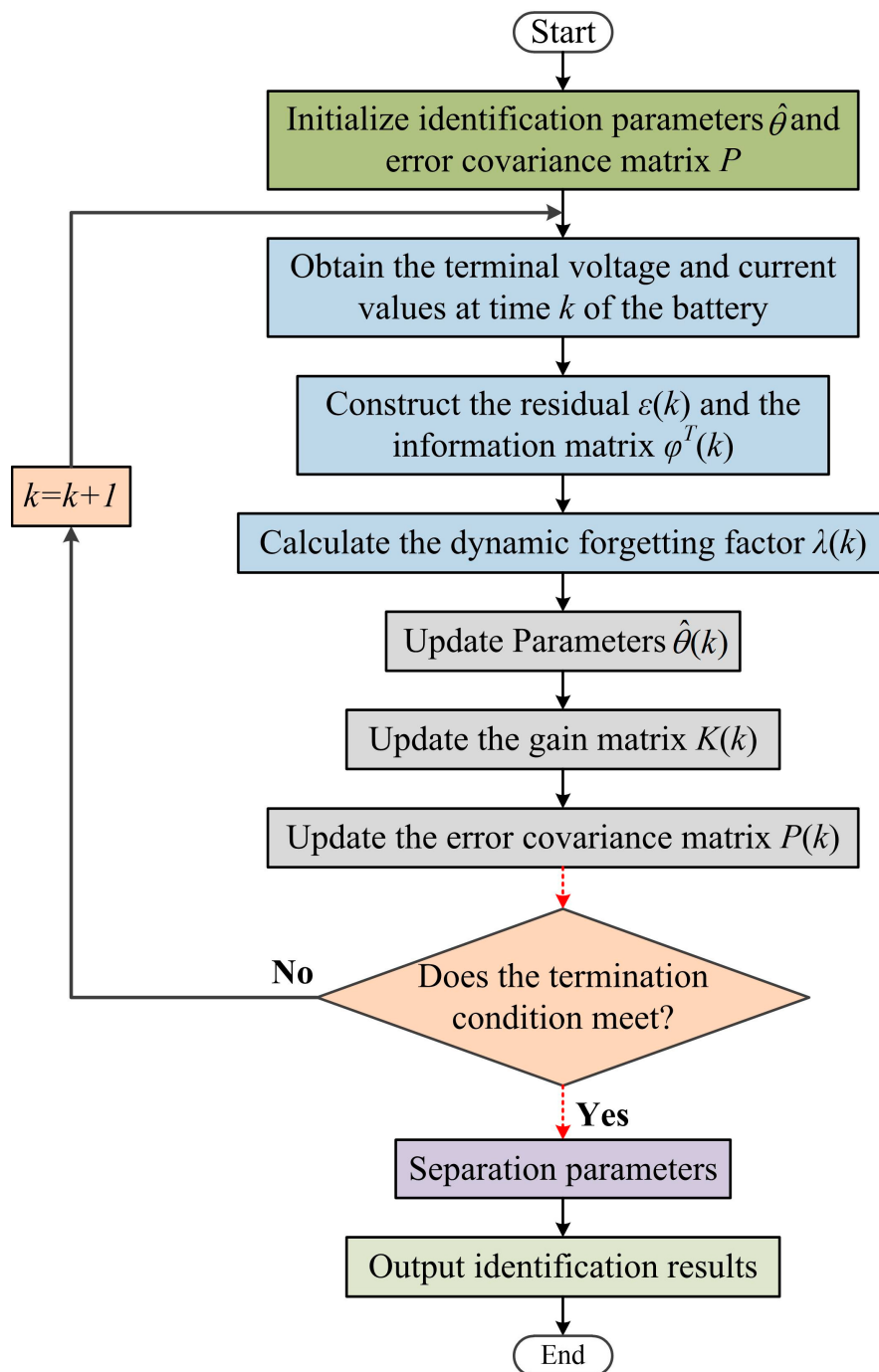


**Figure 4.** Dynamic forgetting factor parameter identification flowchart.

The specific recursive formulas for the DFFRLS method are as follows:

$$\left\{ \begin{array}{l} \hat{\theta}(k) = \hat{\theta}(k-1) + K(k)[y(k) - \varphi^T(k)\hat{\theta}(k-1)] \\ P(k) = \frac{1}{\lambda(k)}[I - K(k)\varphi^T(k)]P(k-1) \\ K(k) = \frac{P(k-1)\varphi(k)}{\lambda(k) + \varphi^T(k)P(k-1)\varphi(k)} \end{array} \right. \quad (15)$$

The parameters of a second-order RC model can be identified online using the DFFRLS method, as illustrated in Figure 5.

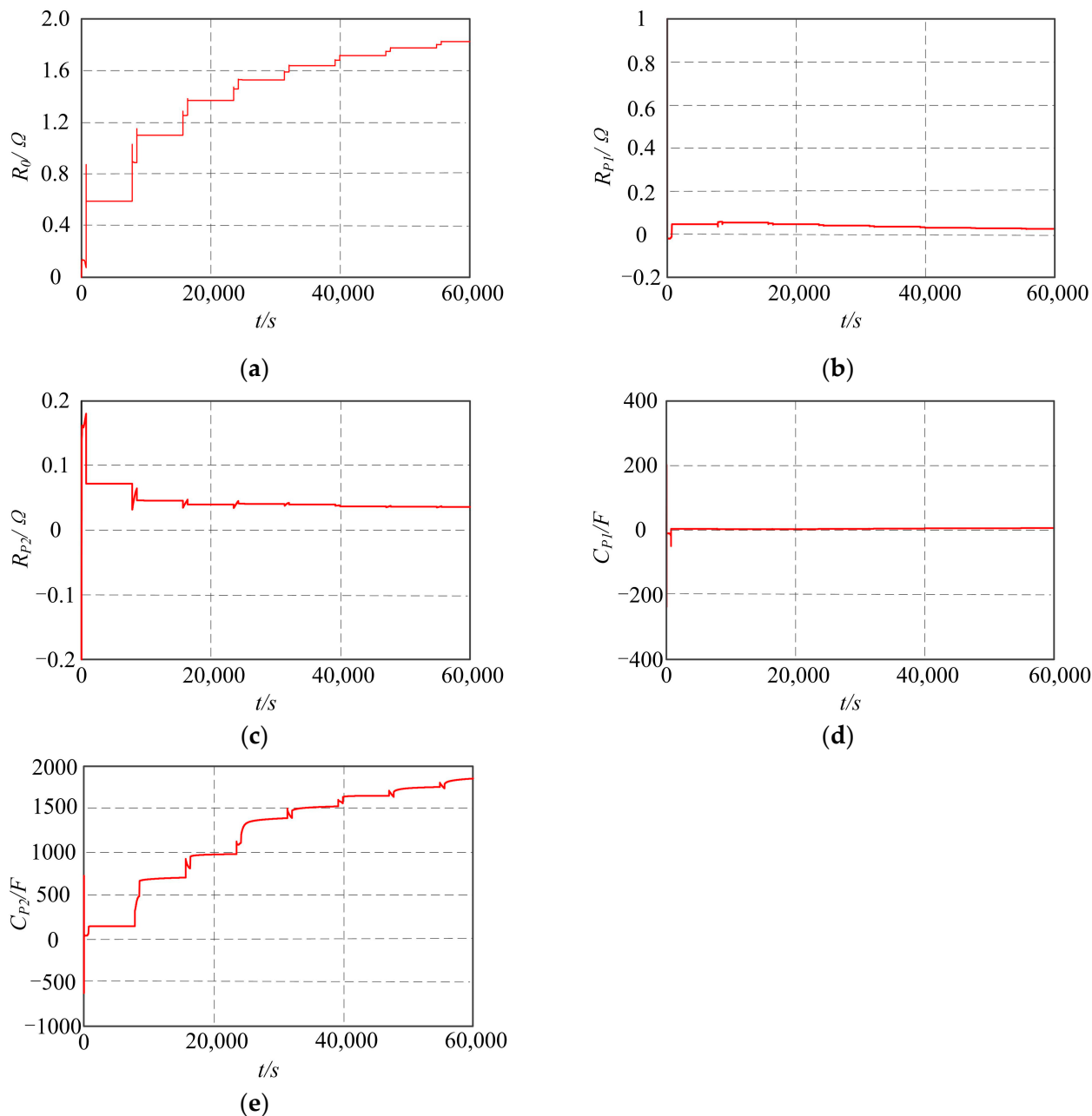


**Figure 5.** Results of battery model parameter identification. (a)  $R_0$ ; (b)  $R_{P1}$ ; (c)  $R_{P2}$ ; (d)  $C_{P1}$ ; (e)  $C_{P2}$ .

#### 4. Research on SOC Estimation Based on Strong Tracking H-Infinity Filtering Algorithm

##### 4.1. H-Infinity Filtering Algorithm

Robust control theory addresses system uncertainties and external disturbances. The H-infinity filtering algorithm does not rely on the noise probability density function to be Gaussian and maintains estimation accuracy despite noise. H-infinity theory, based on game theory, reflects the interplay between the estimation algorithm and noise. The specific steps are as follows. Establish a discrete linear system:

$$\begin{cases} x_{k+1} = A_k x_k + B_k u_k + w_k \\ y_{k+1} = C_k x_k + D_k u_k + v_k \end{cases} \quad (16)$$

In the equations:  $w_k$  and  $v_k$  represent system noise and observation noise, respectively; and  $A_k$ ,  $B_k$ ,  $C_k$  and  $D_k$  are all parameter matrices. The expressions are shown in Equation (17).

$$A_k = \begin{bmatrix} 1 & 0 & 0 \\ 0 & e^{-\frac{\Delta t}{R_{P1}C_{P1}}} & 0 \\ 0 & 0 & e^{-\frac{\Delta t}{R_{P2}C_{P2}}} \end{bmatrix}, B_k = \begin{bmatrix} -\frac{\eta \Delta t}{Q} \\ R_{P1} \left( 1 - e^{-\frac{\Delta t}{R_{P1}C_{P1}}} \right) \\ R_{P2} \left( 1 - e^{-\frac{\Delta t}{R_{P2}C_{P2}}} \right) \end{bmatrix}, C_k = \begin{bmatrix} \frac{\partial U_{oc}}{\partial SOC} \\ -1 \\ -1 \end{bmatrix}, D_k = [-R_0] \quad (17)$$

Using a game theory-based approach, introduce the cost function  $J$ , as shown in Equation (18).

$$J = \frac{\sum_{k=0}^{N-1} \|x_k - X_k\|_{S_k}^2}{\|x_0 - X_0\|_{P_0^{-1}}^2 + \sum_{k=0}^{N-1} (\|w_k\|_{Q_k^{-1}}^2 + \|v_k\|_{R_k^{-1}}^2)} \quad (18)$$

In the equations:  $x_0$  and  $X_0$  are the initial state estimate and set value of the system, respectively;  $Q_k$  and  $P_k$  are the state noise covariance matrix and measurement noise covariance matrix, respectively;  $P_0$  is the initial error covariance matrix.

The goal of H-infinity filtering is to find an estimate  $x_k$  of  $X_k$  such that  $x_k - X_k$  is minimized. Assuming nature as the adversary, contrary to the objective of seeking the optimal estimate, nature always aims to find suitable  $x_0$ ,  $w_k$  and  $v_k$  to maximize  $x_k - X_k$ . Nature can simply make  $x_0$ ,  $w_k$  and  $v_k$  infinitely large to maximize  $x_k - X_k$ , which is obviously unfair. Therefore, when defining the cost function,  $x_0$ ,  $w_k$  and  $v_k$  are placed in the denominator. This means nature must choose appropriate  $x_0$ ,  $w_k$  and  $v_k$  to maximize  $x_k - X_k$ . Similarly, to minimize  $x_k - X_k$  and obtain the optimal estimate, a suitable estimation strategy must be designed. Directly minimizing  $J$  is challenging; hence, an appropriate boundary condition  $\theta$  can be chosen to satisfy:

$$J < \frac{1}{\theta} \quad (19)$$

Substituting Equation (18) into Equation (19) gives the following:

$$J_1 = \sum_{k=0}^{N-1} \left[ \|z_k - \hat{z}_k\|_{S_k}^2 - \frac{1}{\theta} (\|w_k\|_{w_k^{-1}}^2 + \|v_k\|_{v_k^{-1}}^2) \right] - \frac{1}{\theta} \|x_0 - X_0\|_{P_0^{-1}}^2 < 0 \quad (20)$$

Thus, the problem transforms into selecting an appropriate  $X_k$  that minimizes  $J_1$  when  $x_0$ ,  $w_k$  and  $v_k$  maximize  $J_1$ . By solving this problem, we can ultimately find a recursive relation that makes the cost function  $J$  less than  $1/\theta$ , as shown in Equation (21).

$$\begin{cases} K_k = P_k \left[ I - \theta \bar{S}_k P_k + C_k^T R_k^{-1} C_k P_k \right]^{-1} C_k^T R_k^{-1} \\ X_{k+1} = A \hat{x}_k + B u_k + K_k (y_k - \hat{y}_k) \\ P_{k+1} = A P_k \left[ I - \theta \bar{S}_k P_k + C_k^T R_k^{-1} C_k P_k \right]^{-1} A^T + Q_k \end{cases} \quad (21)$$

In this equation:  $K_k$  is the gain matrix;  $P_k$  is the covariance matrix, obtained recursively from the initial covariance matrix  $P_0$ ;  $I$  is the identity matrix; and  $\hat{x}_k$  and  $\hat{y}_k$  are the a priori predicted value and the a priori measured value, respectively.

#### 4.2. Strong Tracking H-Infinity Filtering Algorithm

To enhance system robustness, this section employs a strong tracking filter capable of tracking sudden changes in the system state [37]. The sufficient condition for this filter is the determination of a time-varying gain matrix that satisfies the following two conditions:

- (1) Optimal filter performance.

$$E(x_k - \hat{x}_k)(x_k - \hat{x}_k)^T = \min \quad (22)$$

(2) Output residuals are orthogonal everywhere.

$$E\left(\gamma_k \gamma_{k+j}^T\right) = 0 \quad k = 1, 2, 3, \dots; j = 1, 2, 3, \dots \quad (23)$$

To improve the system's tracking performance for sudden state changes, a reduction factor  $\lambda_k$  is introduced to enhance the weight of current observation data. Thus,

$$\begin{cases} K_k = \lambda_k P_k \left[ I - \theta \bar{S}_k P_k + C_k^T R_k^{-1} C_k \lambda_k P_k \right]^{-1} C_k^T R_k^{-1} \\ P_{k+1} = \lambda_k A P_k \left[ I - \theta \bar{S}_k P_k + C_k^T R_k^{-1} C_k \lambda_k P_k \right]^{-1} A^T + Q_k \end{cases} \quad (24)$$

The value of the fading factor is as follows:

$$\lambda_k = \begin{cases} \lambda_0 & \lambda_0 \geq 1 \\ 1 & \lambda_0 < 1 \end{cases} \quad (25)$$

$$\lambda_0 = \frac{\text{tr}(N_k)}{\text{tr}(M_k)} \quad (26)$$

$$\begin{cases} N_k = V_k - C_k \Gamma_{k-1} Q_{k-1} \Gamma_{k-1}^T C_k^T - \beta R_k \\ M_k = C_k A_k P_{k-1} A_k^T C_k^T \end{cases} \quad (27)$$

$$V_k = \begin{cases} \gamma_1 \gamma_1^T & k = 1 \\ \frac{\rho V_{k-1} + \gamma_k \gamma_k^T}{1+\rho} & k > 1 \end{cases} \quad (28)$$

In the equation:  $V_k$  is the mean square error matrix of the output sequence at time  $k$ ;  $\beta \geq 1$  is the selected weakening factor;  $\Gamma_{k-1}$  is the coefficient matrix of the observation noise; and  $\rho$  is the forgetting factor, typically set to 0.95.

In summary, the strong tracking H-infinity filtering algorithm can be obtained. The proposed STF-HIF flowchart is shown in Figure 6.

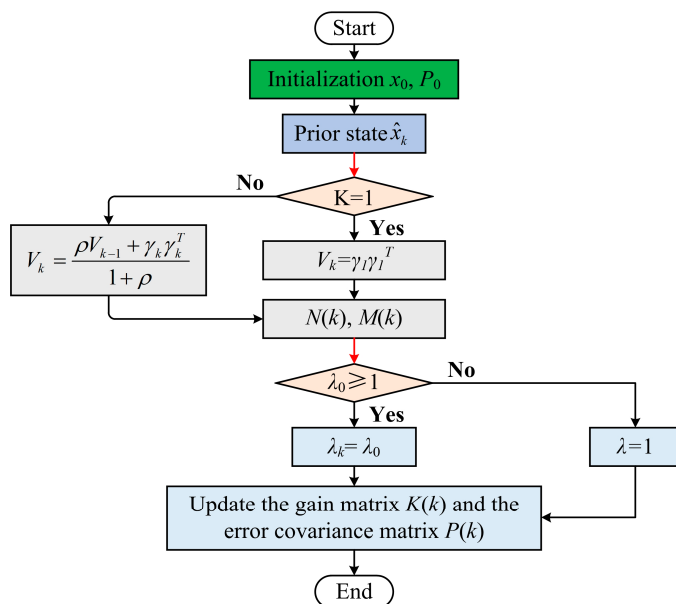


**Figure 6.** Flow Chart of the proposed STF-HIF.

## 5. Experimental Results and Analysis

### 5.1. Analysis of Online Identification Results

To verify the accuracy of the online identification results, the FUDS condition was used as the test condition. The experimental environment was maintained at 25 °C, with

the battery's initial SOC set at 0.8, and the test duration was 10,000 s. The identified parameters were substituted into the second-order equivalent model. The effectiveness of the identification results was validated by observing the deviation between the model voltage and the measured voltage. The simulation results are shown in Figure 7.

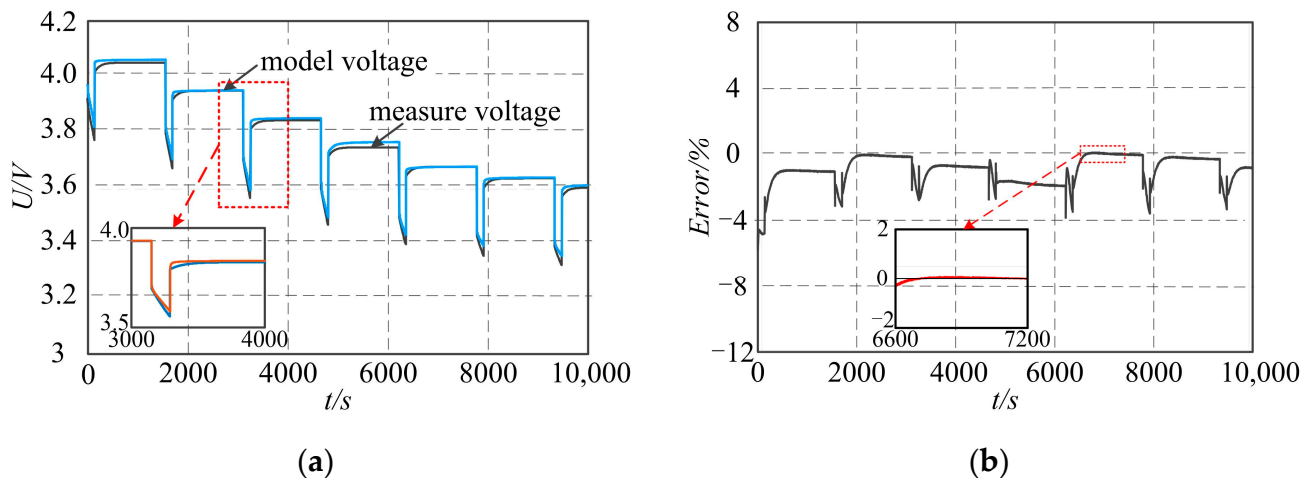


**Figure 7.** (a) Comparison chart of model terminal voltage; (b) Error curve chart.

According to the comparison of the model terminal voltage and the error curve, the deviation between the model voltage and the measured voltage is minimal throughout the entire discharge process. After stabilization, the error remains within 0.06 V. Therefore, the identification results are highly accurate, and the model demonstrates good precision.

### 5.2. Adaptability Analysis of Algorithms under Different Working Conditions

In this study, the working environment temperature is maintained at 25 °C, with the initial SOC set to 80%. The STF-HIF algorithm and the HIF algorithm are used under three conditions: DST, FUDS, and BJDST. The SOC estimates and estimation errors are compared to assess the practical applicability and robustness of the new algorithm.

Under the DST condition, the SOC estimates and estimation errors are shown in Figure 8.

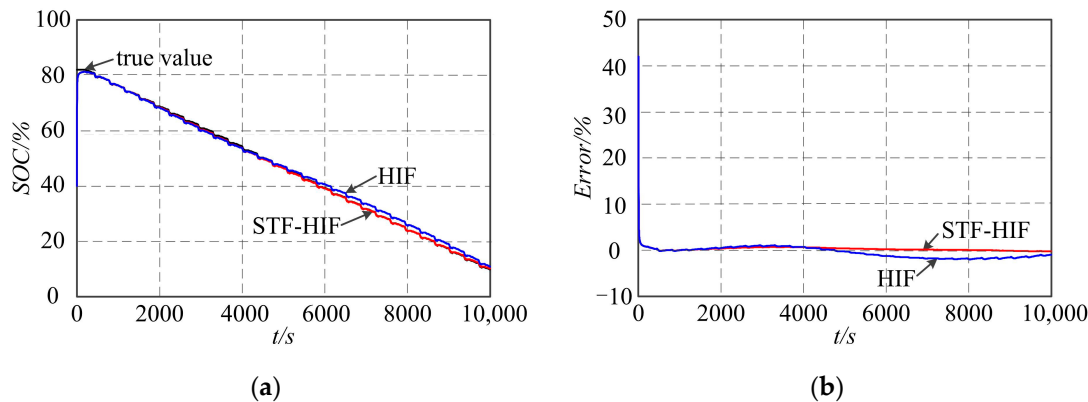


**Figure 8.** (a) SOC estimation under DST conditions; (b) SOC estimation error under DST conditions.

The simulation results indicate that the STF-HIF algorithm's estimates closely align with the true values, with estimation errors remaining minimal and stable. This algorithm demonstrates significantly higher accuracy than the HIF algorithm, with a maximum absolute error of only 0.69%. These results highlight the adaptability of the STF-HIF algorithm and its enhanced practical applicability and robustness for SOC estimation.

Under the FUDS condition, the SOC estimates and estimation errors are illustrated in Figure 9.

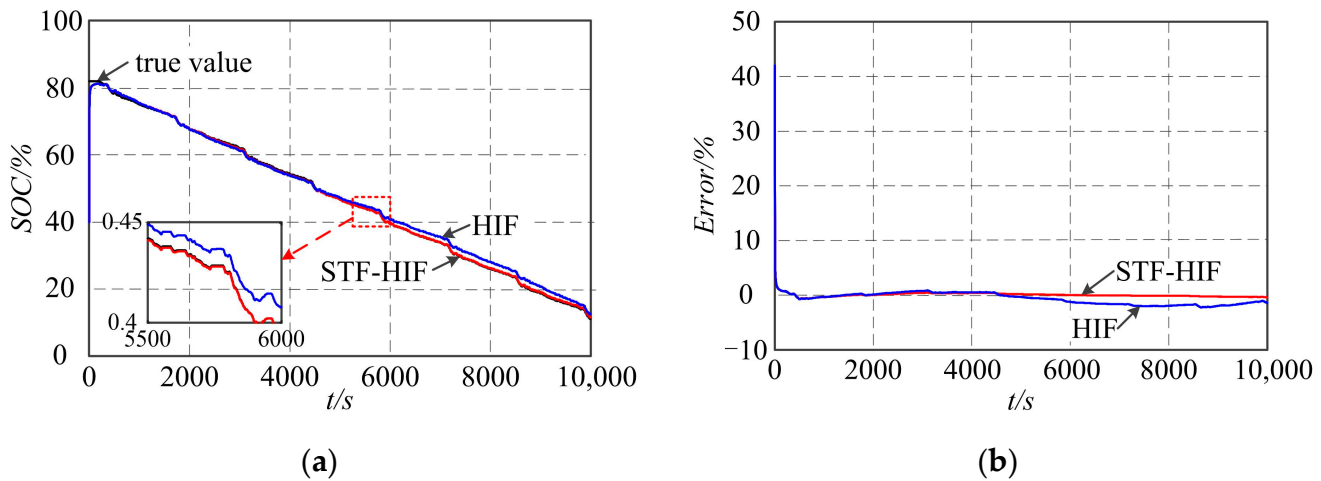


**Figure 9.** (a) SOC estimation under FUDS conditions; (b) SOC estimation error under FUDS conditions.

The simulation results indicate that during the first 5000 s of the discharge process, the estimation accuracy of STF-HIF and HIF is similar. However, as the process continues past 5000 s, the estimation error of HIF gradually increases, while STF-HIF maintains high accuracy. Specifically, the average absolute error of STF-HIF is only 0.25%, demonstrating its robustness and superiority under FUDS conditions. This further validates the practical value of STF-HIF in real-world applications.

Under the BJDST condition, the SOC estimates and estimation errors are illustrated in Figure 10.

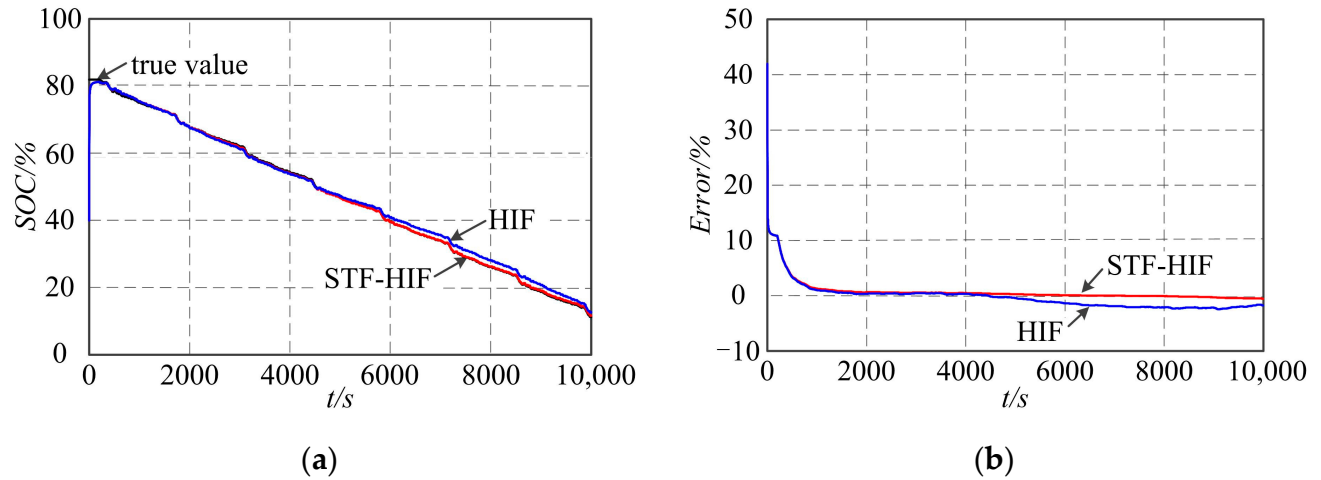


**Figure 10.** (a) SOC estimation under BJDST conditions; (b) SOC estimation error under BJDST conditions.

Based on the above simulations, it is observed that HIF shows a sudden increase in error around 10,000 s of discharge. However, the proposed STF-HIF maintains high accuracy and stability throughout the entire discharge process. Specifically, the root mean square error of STF-HIF is only 0.46%, further demonstrating its superiority and practicality under various conditions. This provides a reliable foundation for the application of SOC algorithms.

A comparison of estimation errors between the STF-HIF and HIF algorithms under DST, FUDS, and BJDST conditions was conducted. Statistical analysis yielded the following conclusions: Compared to the HIF algorithm, the STF-HIF algorithm achieved reductions of 1.34%, 1.56%, and 1.29% in maximum absolute error; reductions of 0.72%, 0.77%, and 0.81% in mean absolute error; and significant reductions of 0.84%, 0.91% and 0.97% in root mean square error. These results indicate a significant improvement in SOC estimation accuracy with the STF-HIF algorithm across different conditions, further validating its superiority in practical applications. Detailed analysis results are presented in Table 3.

**Table 3.** Estimation error under different operating conditions.

Operating Mode	Algorithm	MaxAE%	MAE%	RMSE%
DST	STF-HIF	0.69%	0.27%	0.33%
	HIF	2.03%	0.99%	1.17%
FUDS	STF-HIF	0.72%	0.25%	0.30%
	HIF	2.28%	1.02%	1.21%
BJDST	STF-HIF	1.22%	0.38%	0.46%
	HIF	2.51%	1.19%	1.43%

## 6. Conclusions

This paper focuses on lithium batteries. By augmenting the traditional Thevenin equivalent model with additional parallel RC circuits to create a higher-order equivalent model, it significantly simplifies the dynamic and static characteristics of the battery during charging and discharging, thereby demonstrating strong engineering applicability. To validate the model's effectiveness, the DFFRLS algorithm is utilized for online parameter identification. This approach addresses data saturation issues and ensures rapid convergence and stability of the algorithm. This method integrates the strong tracking filter with the H-infinity filtering algorithm. Experimental results indicate that under DST, FUDS, and BJDST conditions, the STF-HIF algorithm reduces the maximum absolute error by 1.34%, 1.56%, and 1.29%, respectively, compared to the HIF algorithm. Additionally, it decreases the average absolute error by 0.72%, 0.77%, and 0.81%, respectively, and lowers the root mean square error by 0.84%, 0.91%, and 0.97%, respectively. Compared to the traditional  $H_\infty$  filtering algorithm, the improved algorithm significantly enhances the accuracy and robustness of lithium battery SOC estimation. This improvement lays a solid foundation for real-time monitoring and management of battery systems, demonstrating strong practicality.

The parameters of the battery equivalent circuit model are also affected by low temperatures and aging. Future work will focus on online estimation of available capacity and SOC under low temperature and aging conditions to expand the applicability of the proposed method.

**Author Contributions:** Conceptualization, T.Y. and Y.L.; methodology, H.S.; software, Y.L.; validation, T.Y., formal analysis, J.B. and T.Y.; investigation, J.B. and H.S.; writing—original draft preparation, Y.L.; writing—review and editing, J.B. and T.Y.; visualization, H.S.; supervision, H.S.; funding acquisition, T.Y. All authors have read and agreed to the published version of the manuscript.

**Funding:** This research was funded by Scientific Research Project of Education Department of Jilin Province, grant number (No. JJKH20230121KJ).

**Data Availability Statement:** Data are contained with the article.

**Conflicts of Interest:** Author Jing Bai was employed by the company Yuda Engineering (Jilin) Co., Ltd. The remaining authors declare that the research was conducted in the absence of any commercial or financial relationships that could be construed as a potential conflict of interest.

## References

1. Tang, Y. Review on the Application Status and Development of Lithium-ion Batteries in Electric Vehicles. *Environ. Technol.* **2023**, *4*, 94–100.
2. Ren, B.Y.; Sun, J.; Sun, X.D.; Xu, W.N. A simplified second-order model for improving the speed of on-line state of charge estimation of series lithium-ion batteries. *Power Syst. Prot. Control* **2022**, *50*, 110–118. [[CrossRef](#)]
3. Liu, S.Z.; Yuan, L.H.; Zhang, C.; Jin, L.; Yang, Q.X. State of Charge Estimation of LiFeO<sub>4</sub> Batteries Based on Time Domain Features of Ultrasonic Waves and Random Forest. *Trans. China Electrotech. Soc.* **2022**, *37*, 5872–5885. [[CrossRef](#)]
4. Zhang, Z.Y.; Wang, G.S.; Nie, S.X.; Xing, P.X. State of Charge Estimation of LiFePO<sub>4</sub> Battery under the Condition of High-Rate Pulsed Discharge. *Trans. China Electrotech. Soc.* **2019**, *34*, 1769–1779. [[CrossRef](#)]
5. Wang, H.D.; Xu, Y.H.; Zhang, H.G.; Yang, F.F. Review of SOC Estimation Technology for Lithium-ion Power Batteries. *Auto Time* **2023**, *22*, 120–122.
6. Chu, Y.; Li, J.; Gu, J.; Qiang, Y. Parameter identification and SOC estimation of lithium-ion batteries based on AG-COA-ASRCKF. *J. Power Electron.* **2023**, *23*, 308–319. [[CrossRef](#)]
7. Fan, X.M.; Feng, H.; Zhang, X. Optimization of Least Squares Method and Its Application in Parameter Identification of Lithium-Ion Battery Model. *Trans. China Electrotech. Soc.* **2024**, *39*, 1577–1588. [[CrossRef](#)]
8. Zhu, Q.; Li, L.; Hu, X.; Xiong, N.; Hu, G.D. H<sub>∞</sub>-Based Nonlinear Observer Design for State of Charge Estimation of Lithium-Ion Battery with Polynomial Parameters. *IEEE Trans. Veh. Technol.* **2017**, *66*, 10853–10865. [[CrossRef](#)]
9. Dey, S.; Ayalew, B.; Pius, P. Nonlinear Robust Observers for State-of-Charge Estimation of Lithium-ion Cells Based on a Reduced Electrochemical Model. *IEEE Trans. Control Syst. Technol.* **2015**, *23*, 1935–1942. [[CrossRef](#)]
10. Fu, L.; Du, M.X.; Liu, B.; Wei, K.X. Estimation of lithium-ion battery SOC based on combination of open circuit voltage and Kalman filter. *J. Tianjin Univ. Technol.* **2015**, *31*, 9–13.
11. Xiong, R.; He, H.W.; Sun, F.C.; Zhao, K. Evaluation on State of Charge Estimation of Batteries with Adaptive Extended Kalman Filter by Experiment Approach. *IEEE Trans. Veh. Technol.* **2013**, *62*, 108–117. [[CrossRef](#)]
12. Wang, Z.F. State of charge estimation and hardware-in-loop verification of Lithium-ion battery based on BCRLS-AEKF. *Trans. Beijing Inst. Technol.* **2020**, *40*, 275–281. [[CrossRef](#)]
13. Du, B.H.; Zhang, Y.; Wu, T.Z.; He, Y.L.; Li, Z.L. An online identification method for equivalent model parameters of aging lithium-ion bat-tries. *Energy Storage Sci. Technol.* **2021**, *10*, 342–348. [[CrossRef](#)]
14. Pedro, F.; Paul, P.; Pedro, B. On-line parameter estimation of a lithium-ion battery/supercapacitor storage system using filtering sliding mode differentiators. *J. Energy Storage* **2020**, *32*, 101889. [[CrossRef](#)]
15. Feng, F.; Lu, R.; Wei, G.; Zhu, C. Identification and analysis of model parameters used for LiFePO<sub>4</sub> cells series battery pack at various ambient temperature. *IET Electr. Syst. Transp.* **2016**, *6*, 50–55. [[CrossRef](#)]
16. Pavkovic, D.; Krzna, M.; Komljenovic, A.; Hrgetic, M.; Zorc, D. Dual EKF based state and parameter estimator for a LiFePO<sub>4</sub> battery cell. *J. Power Electron.* **2017**, *17*, 398–410. [[CrossRef](#)]
17. Chen, Y.; He, Y.G.; Li, Z. Battery variable temperature model parameter identification by likelihood estimation and SOC estimation. *J. Electron. Meas. Instrum.* **2019**, *33*, 1–9.
18. Ding, Z.T.; Deng, T.; Li, Z.F.; Yin, Y.L. SOC Estimation of Lithium-ion Battery Based on Ampere Hour Integral and Unscented Kalman Filter. *China Mech. Eng.* **2020**, *31*, 1823–1830.
19. Jin, B.W.; Qiao, H.M.; Pan, T.H.; Chen, S. Lithium Battery SOC Estimation Based on Internal Resistance Power Consumption. *Automot. Eng.* **2020**, *42*, 1008–1015+1059. [[CrossRef](#)]
20. Zhang, Y.H. Research on SOC Estimation of Lithium Battery Based on Modified Strong Tracking Filter. Master's Thesis, Tian Jin University, Zhenjiang, China, 2014.
21. Shu, X.; Chen, Z.; Shen, J.; Guo, F.; Zhang, Y.; Liu, Y. State of Charge Estimation for Lithium-ion Battery Based on Hybrid Compensation Modeling and Adaptive H-Infinity Filter. *IEEE Trans. Transp. Electrif.* **2022**, *9*, 945–957. [[CrossRef](#)]
22. Zhao, L.H.; Liu, Z.Y.; Ji, G.H. Lithium-ion battery state of charge estimation with model parameters adaptation using H<sub>∞</sub> extended Kalman filter. *Control Eng. Pract.* **2018**, *81*, 114. [[CrossRef](#)]
23. Chen, Z.; Zhao, H.; Shu, X.; Zhang, Y.; Shen, J.; Liu, Y. Synthetic state of charge estimation for lithium-ion batteries based on long short-term memory network modeling and adaptive H-Infinity filter. *Energy* **2021**, *228*, 120630. [[CrossRef](#)]
24. Liu, F.; Yu, D.; Su, W.; Bu, F. Multi-state joint estimation of series battery pack based on multi-model fusion. *Electrochim. Acta* **2023**, *443*, 141964. [[CrossRef](#)]
25. Dong, G.Z.; Xu, Y.; Wei, Z.B. A Hierarchical Approach for Finite-Time H<sub>∞</sub> State-of-Charge Observer and Probabilistic Lifetime Prediction of Lithium-Ion Batteries. *IEEE Trans. Energy Convers.* **2021**, *37*, 718. [[CrossRef](#)]
26. Chen, C.; Xiong, R.; Shen, W. A Lithium-Ion Battery-in-the-Loop Approach to Test and Validate Multiscale Dual H Infinity Filters for State-of-Charge and Capacity Estimation. *IEEE Trans. Power Electron.* **2018**, *33*, 332–342. [[CrossRef](#)]
27. Liu, Y.; Wang, S.; Xie, Y.; Fernandez, C.; Qiu, J.; Zhang, Y. A novel adaptive H-infinity filtering method f-or the accurate SOC estimation of lithium-ion batteries based on optimal forgetting factor selection. *Int. J. Circuit Theory Appl.* **2022**, *50*, 3372–3386. [[CrossRef](#)]
28. Li, M.; Zhang, Y.; Hu, Z.; Zhang, Y.; Zhang, J. A Battery SOC Estimation Method Based on AFFRLS-EKF. *Sensors* **2021**, *21*, 12. [[CrossRef](#)]

29. Yue, Y.S.; Sun, D.; Xu, S.; Shen, Y.P. Research progress in equivalent circuit model for Li-ion battery. *Battery Bimon.* **2023**, *53*, 682–686. [[CrossRef](#)]
30. Sun, J.L.; Tang, C.Y.; Li, L.; Zhu, J.D.; Zhu, C.B. An Estimation Method of Rechargeable Electric Quantity for Aging Battery Based on Joint Estimation of State and Model Parameters. *Trans. China Electrotech. Soc.* **2022**, *37*, 5886–5898. [[CrossRef](#)]
31. He, J.; Ma, R.F.; Cai, Q.L.; Fan, X.L.; Zhao, W.F.; Deng, Y.L. Life Cycle Identification of Internal Short Circuits of Lithium-ion Battery Based on Recursive Least Square Method. *J. Mech. Eng.* **2022**, *58*, 96–104. [[CrossRef](#)]
32. Hang, R. State of Charge Estimation of Ternary Lithium Battery Based on Variable Forgetting Factor Recursive Least Square Method. Master’s Thesis, Chong Qing University, Zhenjiang, China, 2014.
33. Chen, Z.; Francis, A.; Li, S.; Liao, B.; Xiao, D.; Ha, T.T.; Li, J.; Ding, L.; Cao, X. Egret swarm optimization algorithm: An evolutionary computation approach for model free optimization. *Biomimetics* **2022**, *7*, 144. [[CrossRef](#)] [[PubMed](#)]
34. Wang, D.; Cao, Y.L.; Du, J.L. Parameter identification of Li-ion battery model by MAFFRLS algorithm. *Battery Bimon.* **2024**, *54*, 189–193. [[CrossRef](#)]
35. Calce Battery Research Group [EB/OL]. Available online: <https://web.calce.umd.edu/batteries/data.htm> (accessed on 1 April 2020).
36. Sun, J.L.; Zou, X.; Gu, T.H.; Cui, K.; Zhu, J.D. State of Charge Estimation for Lithium-ion Battery Based on FFRLS-EKF Joint Algorithm. *Automot. Eng.* **2022**, *44*, 505–513. [[CrossRef](#)]
37. Xiong, W.; Mei, H.P.; Xu, G.; Li, Y.H.; Li, Y.M. Lithium-ion battery SOC estimation based on improved H-infinity filter. *Chin. J. Power Sources* **2020**, *44*, 1488–1491+1528.

**Disclaimer/Publisher’s Note:** The statements, opinions and data contained in all publications are solely those of the individual author(s) and contributor(s) and not of MDPI and/or the editor(s). MDPI and/or the editor(s) disclaim responsibility for any injury to people or property resulting from any ideas, methods, instructions or products referred to in the content.